Optimization of the Uniformity of 12-Quad Direct Drive Targets for the National Ignition

Facility

Hanna Wiandt

Pittsford Mendon High School

Advisor: Dr. Stephen Craxton

Laboratory for Laser Energetics

University of Rochester

August 2019

1. Abstract

The National Ignition Facility (NIF) has a total of 192 beams, divided amongst 48 quads located at 23.5˚, 30˚, 44.5˚, and 50˚ from the top and bottom of the target chamber. A proposed experiment requires the use of 24 quads to irradiate a cylindrical hohlraum and 12 quads to compress each of two spherical capsules using direct drive. A sample would be exposed to the high fluxes of x rays and neutrons produced by the hohraum and capsules, respectively. Glass (SiO_2) and plastic (CH) spheres of 1600 µm and 2000 µm diameter were considered for the direct drive capsules. To compensate for the uneven coverage provided by only 12 quads, individual beams were defocused and repointed in the θ (vertical) and φ (horizontal) directions, increasing the uniformity of the imploding capsules. Simulations that varied beam selections, pointings, and defocuses were used to identify an optimum design for each capsule. Nonuniformities as low as 3-4% rms were obtained in all cases.

2. Introduction

Nuclear fusion could one day produce clean energy. One method used to achieve nuclear fusion relies on the irradiation of a capsule using laser beams. The capsule, composed of a spherical shell containing the hydrogen isotopes deuterium and tritium, ablates outward in response to being irradiated. This ablation results in a compressive force inward, creating a high temperature and pressure environment at the core of the capsule. As the hydrogen isotopes are compressed, their strong nuclear forces overcome the repulsive Coulomb forces between them, and the isotopes fuse to form a helium nucleus and an energetic neutron. A fraction of the energy produced by the reaction is redeposited, which in turn leads to more fusion reactions. Provided that there is enough energy redeposited, the fusion reactions can become self-sustaining in a

process known as ignition. The National Ignition Facility (NIF) was built in the hopes of achieving ignition.

      The NIF is capable of depositing laser energy in two processes: direct and indirect drive. A comparison of these two methods can be seen in Figure 1. The former requires that laser beams hit a capsule directly [Fig. 1(a)], whereas the latter utilizes a cylindrical container referred to as a hohlraum [Fig. 1(b)]. The hohlraum allows laser beams to enter through openings located at the top and bottom of its structure, and emits x rays when irradiated by laser energy. It is these x rays which then compress the capsule. While this allows for more uniform compression, the energy absorbed in the process of creating x rays, coupled with the loss of energy through the openings, make indirect drive much less energy efficient than direct drive.
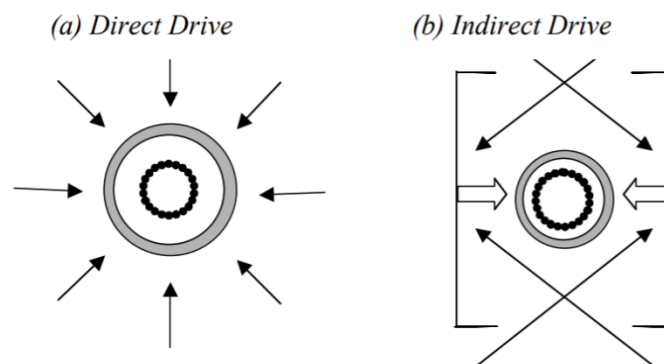

Figure 1. Two approaches to nuclear fusion using lasers. (a) Direct drive uses laser beams (shown here as thin arrows) to irradiate a capsule directly. (b) Indirect drive relies on a hohlraum to produce x rays (shown here as thick arrows), which then compress the capsule. (From Ref. 1)

      The NIF was originally intended for indirect drive. Accordingly, its beam ports are located in four rings at angles θ of 23.5°, 30°, 44.5°, and 50° from the vertical in the upper and lower hemispheres. Because they rest at such a great angle from the equator, its beams have to be repointed in order for the NIF to achieve direct drive. The locations of beams and the necessary

adjustments can be seen in Figure 2. The beams cannot simply be pointed towards the center of the capsule. Doing so would place much more energy near the poles than the equator, resulting in uneven compression and a compromised neutron yield. To ensure a successful experiment, then, some beams have to be repointed towards the equator, in a process known as polar direct drive.[2,3]
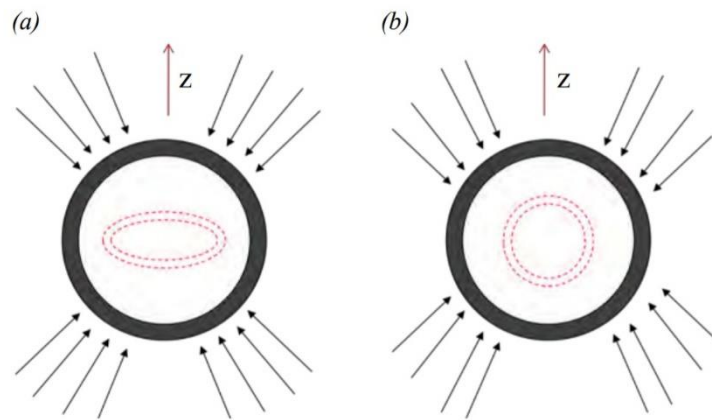

Figure 2. NIF beam pointings (thin arrows) and resultant compression pattern of the capsule (pink rings). (a) If the laser beams are pointed towards the center of the capsule, uneven energy deposition results in a flat compression. (b) Polar direct drive compensates for beam placements by repointing beams towards the equator for a more uniform compression. (From Ref. 4)

As a high amount of energy is being deposited by laser beams in direct drive, a plasma forms around the capsule. This plasma, a gas which contains both ions and electrons, is comparable to the conditions found in space. By mimicking the densities, temperatures, and pressures found in stars, the NIF serves as a way to bring distant phenomena into a laboratory environment. Neutrons and x rays from fusion experiments can also be applied to observe the reaction of materials to large amounts of energy.

The combined environment target was proposed by Dr. Yeamans of Lawrence Livermore National Laboratory as a means of studying a sample's reaction to x rays and neutrons.[5] The 48

quads of the NIF are divided into three groups, providing energy to a hohlraum and two spherical
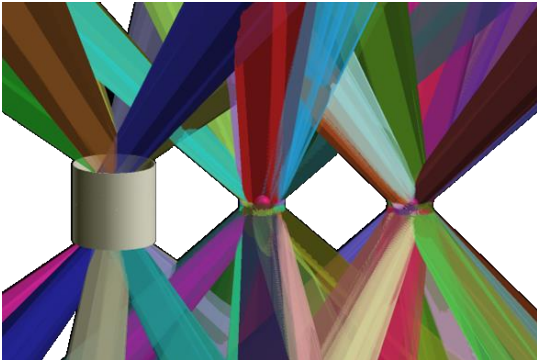
capsules, as shown in Figure 3.

Figure 3. Laser beams being used to irradiate a cylindrical hohlraum and two spherical capsules. (From Ref. 5)

The irradiation of the hohlraum produces x rays, in a fashion similar to indirect drive.

Unlike indirect drive, however, the hohlraum does not contain a capsule, as the objective of the

hohlraum is solely that of producing x rays. The compression of the two spherical capsules in

direct drive produces neutrons. While the number of quads required for each target is fixed—24

quads for the hohlraum and 12 for each direct drive target—the division of the quads can vary.

It is important that the spherical capsules implode as evenly as possible, to maximize

their neutron yield. However, with the use of only a quarter of all the NIF's quads for each

capsule, large areas of the target surface can easily be left with less compression than average,

while other regions become over compressed. In this work, combined environment targets were

designed, with plastic (CH) and glass (SiO_2) capsules, in 1600 µm and 2000 µm diameter sizes,

for two different sets of quads. The pointings and defocuses of each beam were adjusted to

optimize implosion uniformity, with each capsule achieving uniformities between 3-4% rms.

3. Factors that Influence the Implosion

The beam selection, laser pulse shape, and beam pointings and defocuses of an

experiment on the NIF are discussed in Sections 3.1-3.3, respectively, as they contribute to the

uniformity of a capsule's implosion. The beam selection determines the locations of beams

relative to the target surface. The laser pulse shape determines the amount of energy delivered to a capsule. Lastly, the beam pointings and defocuses increase the uniformity of a capsule's implosion by distributing energy in certain patterns.

3.1 Beam Selection

The NIF has eight rings of quads, with four rings each in the upper and lower hemispheres. Figure 4 shows the layout of quads relative to a capsule on the NIF. The whole surface of the capsule can be seen, with lines of constant θ and φ indicated by dashed lines. For each direct drive target, there need to be six quads from each of the upper and lower hemispheres of the NIF. Of these six, two have to be inner quads (from rings 1 and 8 in Figure 4), and four have to be outer quads (from rings 4 and 5 or 3 and 6). This division between upper and lower hemispheres allows for similar configurations to be used for each capsule, and helps to achieve a uniform compression. Alternating quads were used in both inner and outer rings, for optimal azimuthal symmetry. The selection of quads from rings 4 and 5 was limited by the architecture of the NIF; certain 50º quads—those shown in Figure 4 as colorless—are linked to 30º quads in such a way that they must be fired simultaneously. It was therefore decided that quads from rings 2 and 7 (the 30˚ quads) would be reserved for the irradiation of the hohlraum, along with the 50˚ quads that they are linked to.

This reduces the number of available 50˚ quads in such a way that if one capsule were to use 50˚ quads, the other would have to use 44.5˚ quads. As these quads are even further from the equator, the nonuniformity of implosions at the equator is magnified. This makes designs using the 44.5˚ quads especially challenging.
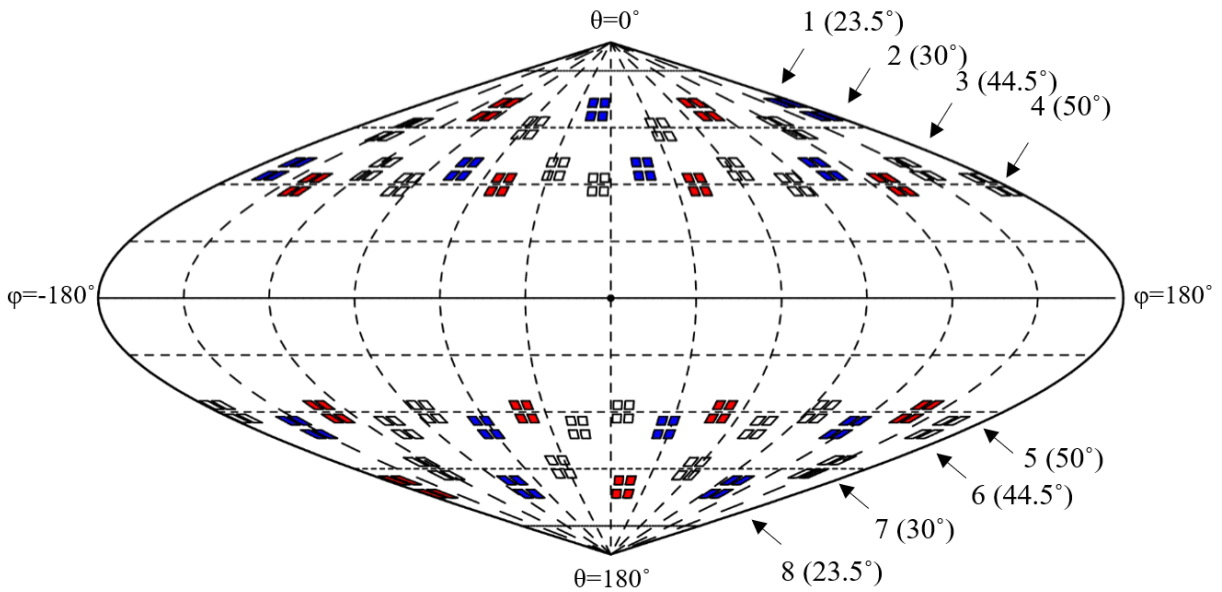
Figure 4. One option for division of NIF quads among direct drive targets. In the configuration shown, the quads irradiating capsule 1 are marked in red and those irradiating capsule 2 in blue. The colorless quads irradiate the hohlraum. Rings have been labeled 1-8.

3.2 Laser Pulse Shape

To avoid damaging the optics of the NIF and thus lower the cost of a shot, a maximum total energy of 534 kJ was selected. Each group of 12 quads would therefore require 133.5 kJ. This led to the laser pulse shown in blue (incident) in Figure 5. To determine the maximum power, P_{max}, of the laser pulse required to deliver this amount of energy, the following equation was used, where P represents power, E energy, and t time:

$$E = \int Pdt = \frac{1}{2}\left(t_4 + (t_3 - t_2)\right)P_{max} \tag{1}$$

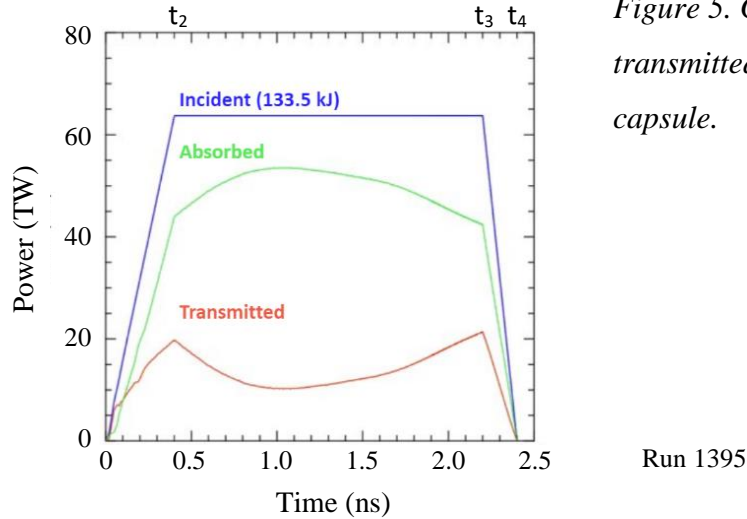The times t_2-t_4 from Eq. (1) can be seen in Figure 5.

Figure 5. Graph of incident, absorbed, and transmitted power delivered to a spherical capsule.

Run 1395

The time t_2 was taken to be 0.4 ns to allow the laser adequate time to reach the maximum power desired, t_4 was set at 2.4 ns, and t_3 had to be 0.2 ns less than t_4, to allow the laser enough time to power down. Substituting into Eq. (1), the maximum power was found to be 63.75 TW for each group of 12 quads, which is comfortably less than the 112.5 TW that the NIF is capable of.

Furthermore, as the shape of the laser pulse and the amount of energy delivered to the capsule had been set, each capsule's shell thickness served as a valuable variable for adjusting the implosion time of the capsule, with thinner capsules imploding faster. To minimize wasted laser energy, the implosion would ideally occur towards the end of the laser pulse, between 2.2 ns and 2.4 ns. The energy that is deposited onto the surface of the capsule becomes absorbed energy, while the energy that continues past the capsule becomes transmitted energy, which risks causing damage to the optics of the NIF if it is too large. A later implosion therefore allows for more absorbed and less transmitted energy.

3.3   Beam Shifting and Defocusing

Each of the individual beams on the NIF can be repointed to a specific location on the

initial capsule surface determined by the angles θ and φ, and can also be defocused by adjusting

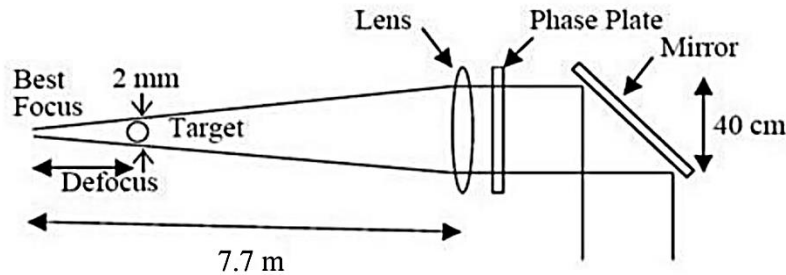the distance of the focus lens to the capsule [Figure 6].

Figure 6. Diagram (not to scale) representing the defocusing and pointing mechanisms of a laser beam. Defocus can be adjusted by moving the lens closer to or further from the capsule along the axis of the laser beam. Changing the angle of the mirror controls beam pointing. (From Ref. 4)

These three parameters function as a means of controlling the pattern of energy

deposition on the surface of a direct drive target. Repointing a beam allows for a different area

on the surface of the capsule to be irradiated. Defocusing a beam changes its focal point, hence

altering the size and intensity of the beam spot. Using only 25% of the beams of the NIF for a

capsule increases the risk of uneven energy deposition, which can greatly compromise the

neutron yield of an experiment. Therefore, finding the optimum beam pointings and defocuses is

especially important.

4. Sample Optimized Design

The aim of the optimization process was to develop compatible designs that would

implode at an optimum time with maximum uniformity, using only 12 NIF quads each. The time

when peak density occurs can be used to define the implosion time, as there is no precise

moment when the capsule implodes. Thus, the implosion time was determined by graphs of the maximum density of the capsule plotted versus time [Figure 7].
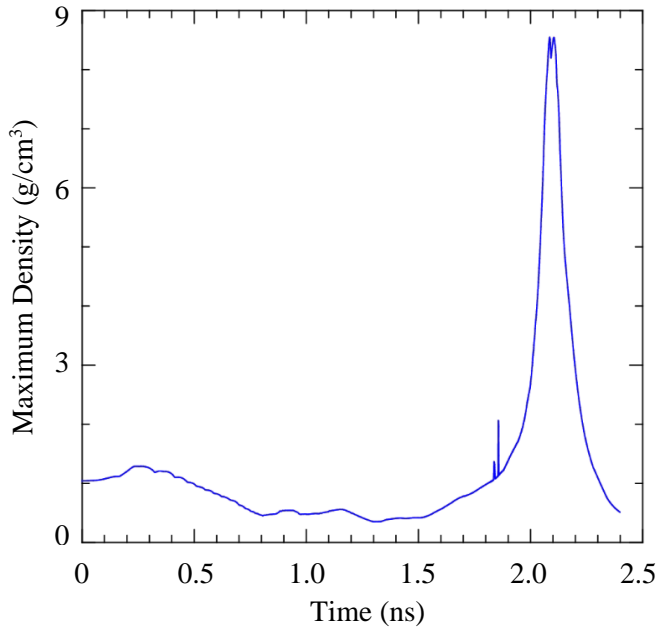

Figure 7. Plot of maximum density versus time in an optimized design. Peak density occurs at 2.1 ns, indicating that the implosion will happen near the ideal 2.2-2.4 ns range.

Run 1162

Using such graphs, optimum thicknesses were determined for glass and plastic capsules in 1600 µm and 2000 µm diameters. These thicknesses, and the corresponding implosion times, can be seen in Table 1. All of the thicknesses are reasonable in terms of manufacturability, and would be capable of holding the required pressures of hydrogen isotopes. The capsules also implode late enough in the laser pulse to reduce transmitted energy to an amount that would not damage the optics of the NIF.

Table 1. Comparison of shell thicknesses and implosion times for four capsule designs with two quad selections.

Capsule	Thickness (µm)	Implosion time (ns)	
		50˚ quads	45˚ quads
1600 µm glass	8	2.15	2.4
1600 µm plastic	14	2.1	2.35
2000 µm glass	5	2.1	2.3
2000 µm plastic	10	2.1	2.3

The 1600 μm diameter glass capsule with a shell thickness of 8 μm, using 50˚ quads, was chosen as a sample case for initial study, and is discussed in the remainder of this section, while the other designs are reserved for Section 5. Both the azimuthal and vertical directions were considered to determine uniformity during optimization. The use of 2-D hydrodynamic simulations, run using the code SAGE, allowed for comparisons between models with different beam groupings, pointings, and defocuses. The basic effects of adjustments can be seen in raytrace plots of the capsule implosion, which display density contours as the implosion progresses [Figure 8]. The shell expands as the capsule implodes, creating an area of higher density towards the center of the capsule. These simulations average the density of an imploding capsule in the azimuthal direction. The more circular the density contours, the more spherical the implosion.

The rays from a $\theta=50$˚ beam are plotted as red lines in Figure 8. Once a ray has deposited 99% of its energy, the line representing it stops. Hence, any lines that continue on, curving away from the capsule, represent rays that possess at least 1% of their original energy. The energy deposited onto the capsule by the rays contributes to the absorbed energy graphed in Figure 5, whereas any energy carried beyond the capsule becomes transmitted energy. The further from its angle of origin that a beam is pointed, the less of its energy is absorbed by the capsule. This leads to the rebounding of the rays that are closest to the equator in Figure 8. Energy absorption is further weakened when 44.5˚ beams are used as opposed to 50˚ beams, due to the fact that 44.5˚ beams pointed towards the equator are repointed a greater θ from their angle of origin than 50˚ beams. This leads to the difference in implosion times seen in Table 1; 44.5˚ capsules implode slower because they absorb less energy.
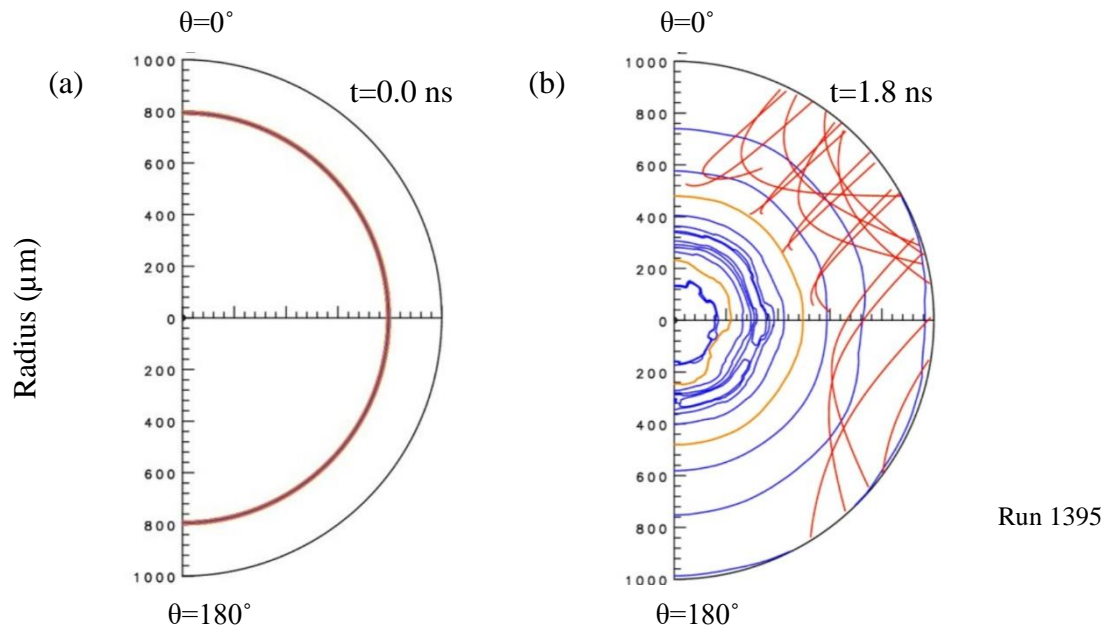
Figure 8. Two raytrace plots depicting the implosion of a 1600 μm diameter glass capsule with shell thickness 8 μm. (a) The capsule prior to implosion is spherical in shape. (b) As the capsule implodes, it compresses inwards, remaining as similar as possible to its initial spherical shape as a result of beam placement. At 1.8 ns, the capsule has imploded just past 400 μm, half of its initial radius. The red lines represent laser rays from a beam incident at θ=50˚. The blue lines are density contours, while the yellow lines represent critical density (the maximum density that the laser can reach).

For each radial line in these 2-D raytrace plots, from θ=0˚ to 180˚, the center-of-mass radius was calculated. This was then plotted as a function of θ in Figure 9 to more clearly illustrate the differences in nonuniformity between unoptimized and optimized designs. This radius was averaged over all φ. The root-mean-square (rms) deviation from the average radius averaged over all angles was calculated to compare nonuniformities. The graph on the left shows an unoptimized design, while the graph on the right is for a final, optimized model of the implosion for the same capsule. As can be seen in the first graph, Figure 9(a), the initial design has a larger center-of-mass radius at the equator than at the poles, indicating that the capsule is

losing its spherical shape and compressing into a flatter mass. The final graph, Figure 9(b), which corresponds to Figure 8(b), is much more uniform, displaying a more even radius throughout the shell and therefore indicating a more uniform, spherical implosion. These differences are owed to adjustments in beam pointings and defocusing. To compensate for the protrusion at the equator in Figure 9(a), beams were pointed further towards the equator. Simultaneously, to slow the compression of the capsule near the poles, the beams closest to the poles were given larger defocus distances. Between these two models, the use of different beam pointings and defocuses reduced the rms from 2.59% to 1.00% in the vertical direction.
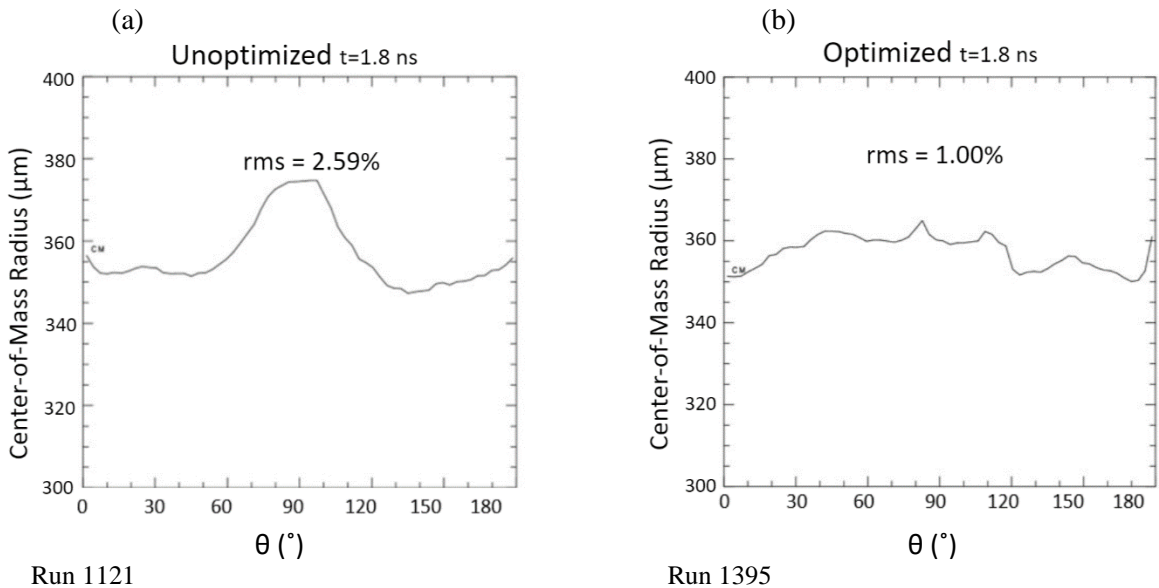

Figure 9. Graphs of center-of-mass radius with respect to the angle θ from the z axis for an initial design (a) and a final design (b) .

The extent of azimuthal nonuniformity is more clearly illustrated by 3-D center-of-mass profiles like Figure 10, which display the distribution of compression on the three dimensional surface of the capsule projected onto a two dimensional profile.[4] SAGE calculates both the azimuthally averaged center-of-mass radius [Fig. 9] and the rays' three dimensional distribution

of energy onto the target surface. At each θ, SAGE adjusts the center-of-mass radius in the φ direction to be consistent with the variations in φ of energy deposition onto the capsule. In Figure 10, which is an initial attempt at optimization, areas in red have compressed further than areas in blue. The quads being used to irradiate the capsule, shown here in green, correspond to the quads marked in red in Figure 4. Each black dot represents the aim point of a laser beam. However, even with the dispersal of aim points, a laser beam still deposits much of its energy near its point of origin. The use of only 12 quads for each capsule, therefore, distributed the laser energy in such a way that large areas of the capsule were left with less compression. Simply spacing the equatorial aim points evenly did not lead to even compression. The 3-D rms of Figure 10, which was calculated similarly to the rms of Figure 9, except averaged over the whole sphere, was determined to be 5.07%.
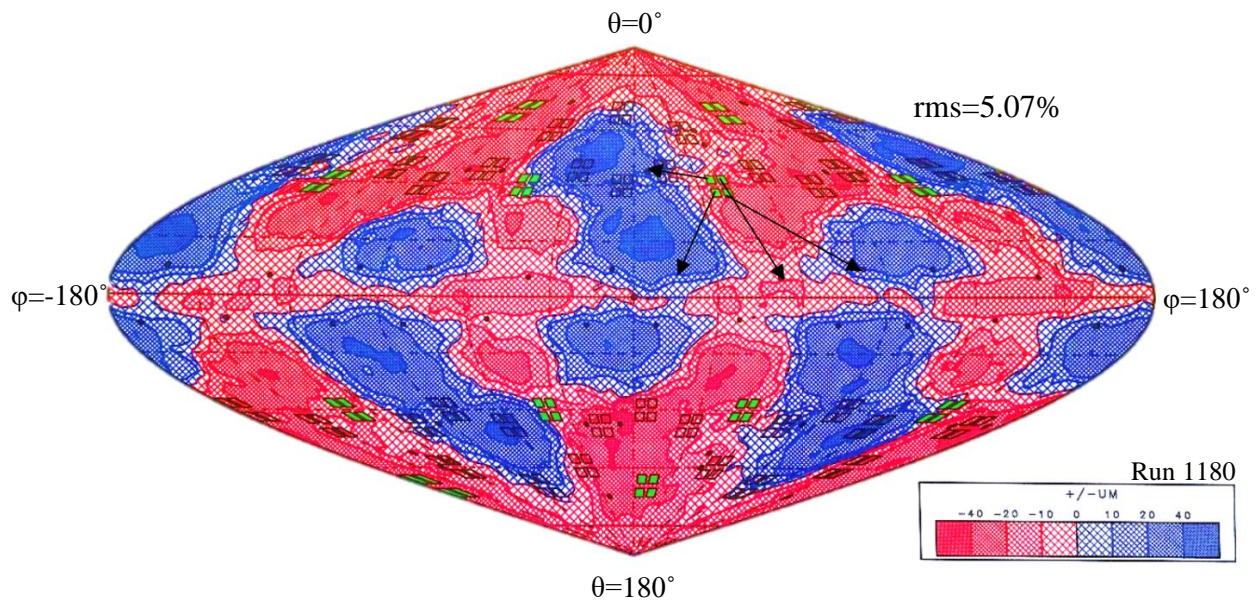

Figure 10. 3-D center-of-mass profile (contours corresponding to the deviation of the center of mass from the average in μm) of a 1600 μm diameter glass capsule at 1.8 ns. Areas in red have compressed further than areas in blue. The quads being used for this capsule, marked in green, correspond with the areas of greatest compression. Black dots represent aim points.

To compensate for the large swathes of red shown above, each beam in a 50˚ quad was pointed further outward from its point of origin, bridging the gaps in between active quads. As the beams were moved further to either side, a different pattern emerged, indicating a more uniform capsule implosion with an rms of 2.82% [Figure 11]. The equatorial aim points have moved further outwards; they are no longer evenly spaced, as they were in Figure 10. The areas of greatest compression have thus shifted and diminished, with the areas in red changing from thick vertical patches to narrower, slanted regions. As Figures 10 and 11 are on the same scale, it can also be seen that the dark red and blue patches are not as dark, nor as large, in Figure 11 indicating that there is less variation in compression than in Figure 10.
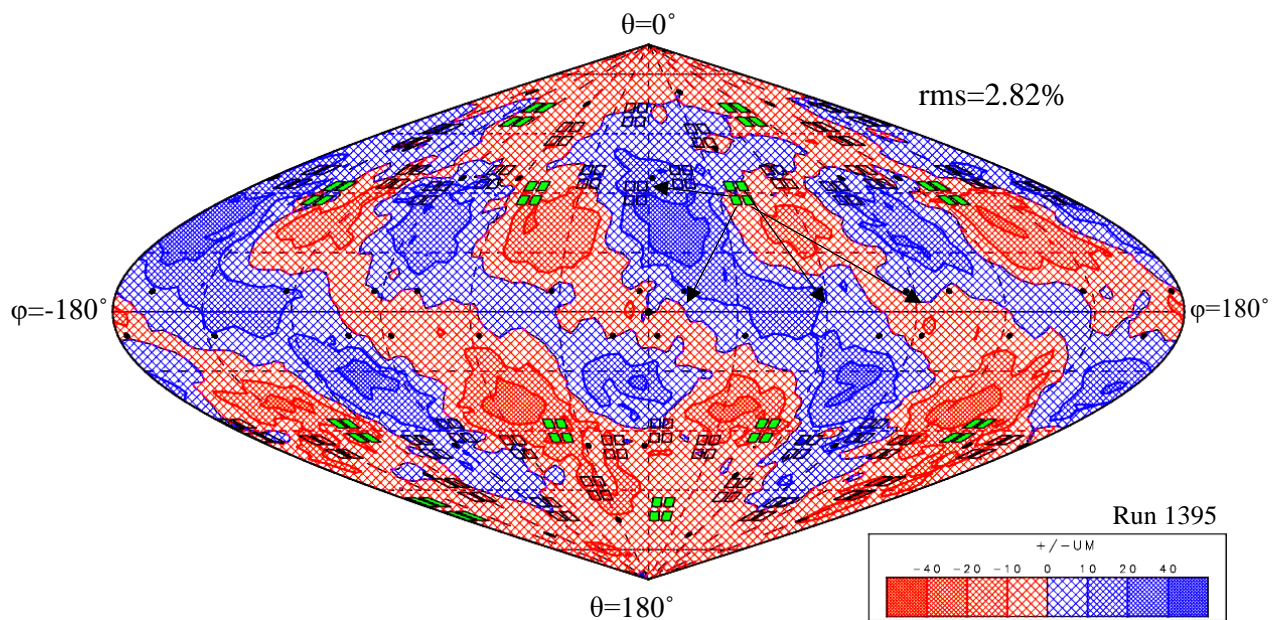

Figure 11. 3-D center-of-mass profile of a 1600 μm diameter glass capsule with adjusted beams at 1.8 ns.

5. Set of Optimized Designs

The approach from this model was then applied to the other cases listed in Table 1. In order to run the experiment, two compatible designs—that is, one 44.5˚ and one 50˚ capsule—

need to have acceptable nonuniformities. The most successful designs for the two 1600 µm glass

capsules are shown in Table 2 and Figure 12. Figure 12 is a pictorial representation of the aim

points specified for the 50˚ capsule detailed in Table 2. θ_0 refers to the angle of origin of the

quad, while θ_1 is the angle to which the beam has been pointed. For the 50˚ capsule, any beam

pointed towards the poles was given a defocus of 1.4 cm, while those pointed towards the

equator were given a defocus of 1 cm. This prevented the poles of the capsule from being

overdriven and compressing faster than the equator. The beams that were pointed towards the

equator were actually pointed either 7˚ or 8˚ above or below it (no beams were pointed over the

equator, as this would have greatly increased transmitted energy), instead of directly at the

equator, to prevent the equator from compressing in a localized band.

Table 2. Optimized beam pointings and defocuses for two capsules. These are all the specifications needed to set up the laser. Both capsules are 1600 µm diameter glass. Each beam is labeled as follows: ring number-top(A)/bottom(B)-left(L)/right(R). Each quad in a ring followed the same specifications.

| 50˚ capsule			Run 1395		44.5˚ capsule			Run 1308
beam	θ_0 (˚)	θ_1 (˚)	$\Delta\varphi$ (˚)	defocus (cm)	beam	θ_0 (˚)	θ_1 (˚)	$\Delta\varphi$ (˚)	defocus (cm)
1A-L	23.5	16	-35	1.4	1A-L	23.5	45	-32	2.3
1A-R	23.5	20	35	1.4	1A-R	23.5	20	32	2.3
1B-L	23.5	35	-35	1.4	1B-L	23.5	40	-32	2.3
1B-R	23.5	45	35	1.4	1B-R	23.5	45	32	1.2
4A-L	50	45	-35	1.4	3A-L	44.5	45	-32	1.2
4A-R	50	83	15	1	3A-R	44.5	90	12	1.2
4B-L	50	83	-25	1	3B-L	44.5	90	-22	1.2
4B-R	50	83	45	1	3B-R	44.5	90	42	1.2
5A-L	130	98	-45	1	6A-L	135.5	90	-42	1.2
5A-R	130	98	25	1	6A-R	135.5	90	22	1.2
5B-L	130	98	-15	1	6B-L	135.5	90	-12	1.2
5B-R	130	135	35	1.4	6B-R	135.5	135	32	1.2
8A-L	156.5	135	-35	1.4	8A-L	156.5	135	-32	1.2
8A-R	156.5	145	35	1.4	8A-R	156.5	140	32	2.3
8B-L	156.5	160	-35	1.4	8B-L	156.5	160	-32	2.3
8B-R	156.5	165	35	1.4	8B-R	156.5	135	32	2.3
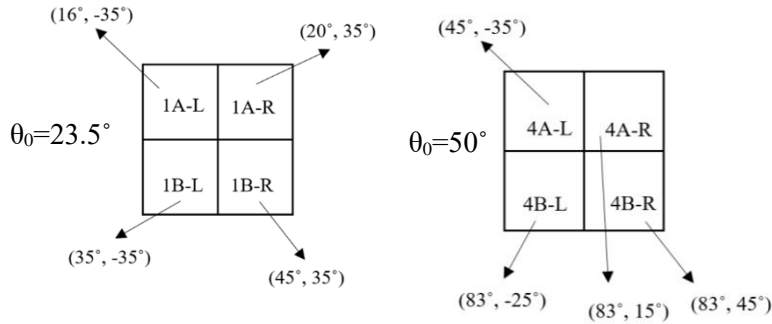
Figure 12. Diagram of pointings of individual beams in two quads for the 50˚ capsule of Table 2.

In the 44.5˚ case, to compensate for their increased distance from the equator, beams were pointed directly at the equator, as opposed to just above or below it. Beams were also given larger defocus distances, so that they would distribute less of their energy in concentrated areas. The three beams closest to the poles for the 44.5˚ capsule have a defocus of 2.3 cm, while all others have a defocus of 1.2 cm. This resulted in the 3-D center-of-mass profile seen in Figure 13.
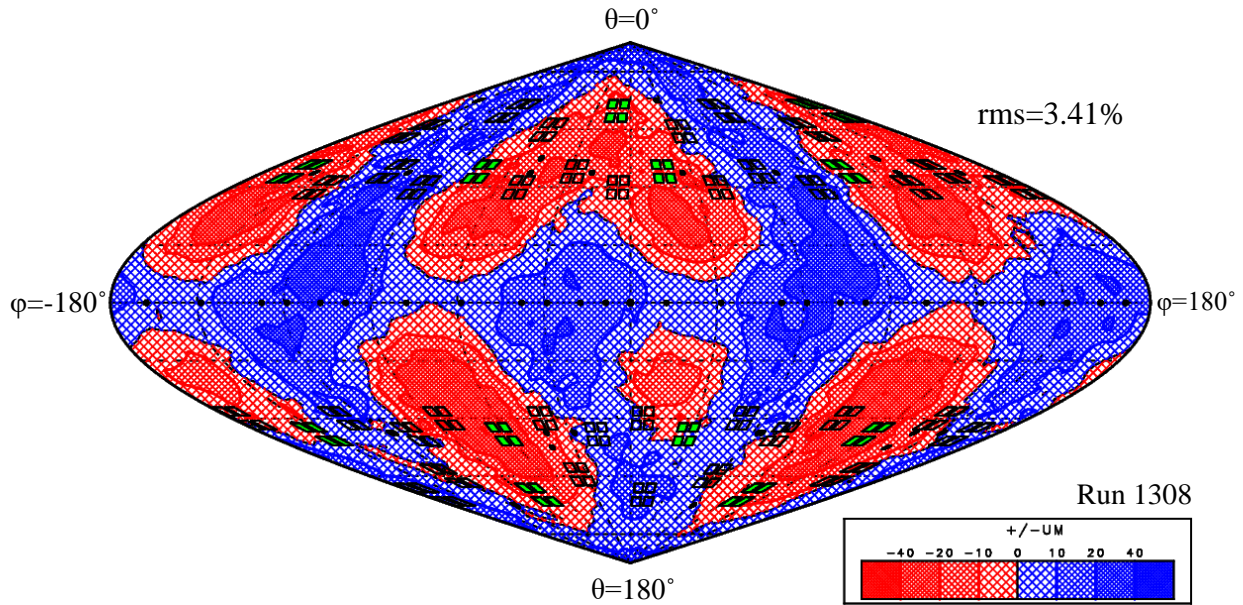

Figure 13. 3-D center-of-mass profile of a 1600 μm diameter glass capsule irradiated with 44.5˚ quads at 1.8 ns.

While Figure 13 does not seem as uniform as Figure 11 visually, the differences in their rms deviations are small, with Figure 11 having an rms of 2.82% and Figure 13 having an rms of

17

3.41%. In the case of the 44.5˚ capsule, the over compressed regions did not cross the equator as they did in the 50˚ case, due to the increased distance of the 44.5˚ quads from the equator. These over compressed regions also tended to be more concentrated, as the 44.5˚ and 23.5˚ quads are closer to one another than the 23.5˚ and 50˚ quads. The areas of over compression therefore correspond with the areas where the greatest number of quads are in closest proximity to one another.

   The rms for all cases is shown in Figure 14. Although the use of 44.5˚ quads did not achieve quite as uniform implosions as the use of 50˚ quads, with an average 0.35% rms difference between corresponding capsules, all capsule nonuniformities achieved rms deviations as low as 3-4%.
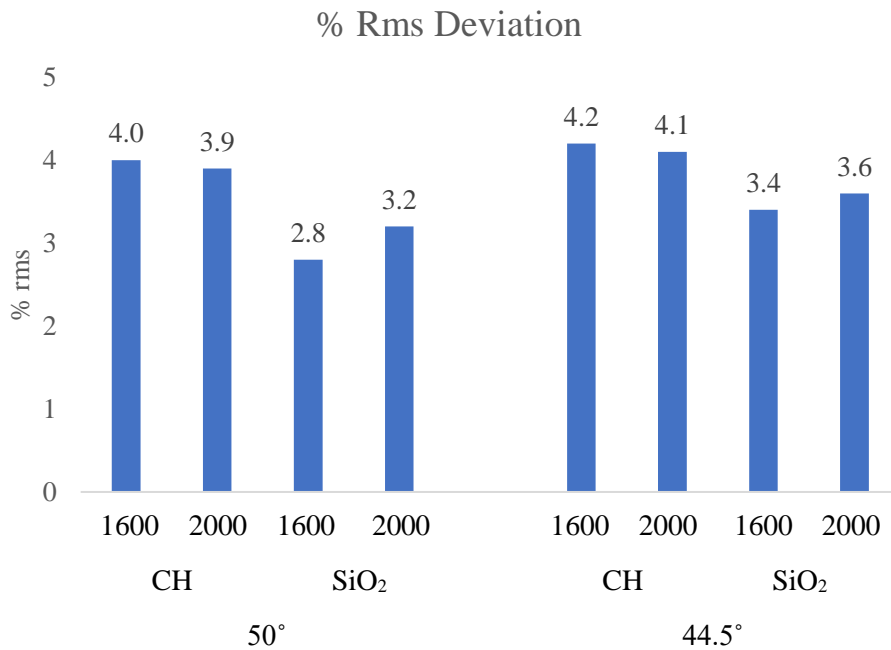
Runs 1455, 1490, 1395, 1437, 1367, 1354, 1308, 1303

Figure 14. Bar graph comparing nonuniformities at 1.8 ns of eight models, categorized by size (in μm), composition, and beam configuration.

The absorbed energies, shown in Figure 15, result from the size, composition, and beam selection of each capsule. 50˚ capsules, for example, have higher absorbed energies than 44.5˚ capsules, because the beams pointed towards the equator do not have to travel as far from their point of origin. Plastic capsules tend to absorb energy less efficiently than glass capsules, as absorption increases with atomic number, which is larger for Si and O than for C and H. Capsules of larger diameter absorb more energy than smaller ones, because laser rays travel a greater distance through the plasma around the capsule. The differences in implosion time between a 44.5˚ and 50˚ capsule [Table 1] are due to the differences in absorbed energy; a target that absorbs more energy implodes sooner than one that absorbs less.
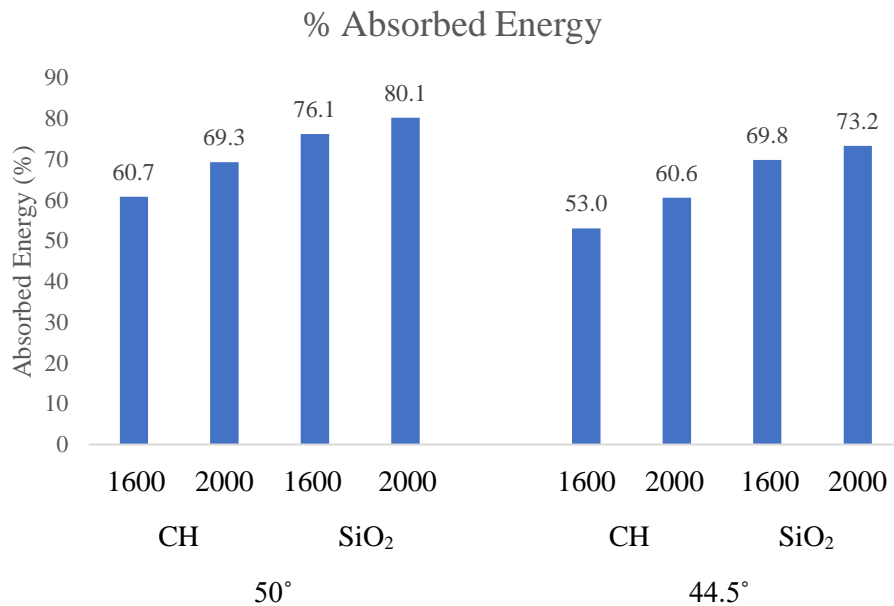
Runs 1455, 1490, 1395, 1437, 1367, 1354, 1308, 1303

Figure 15. Graph of absorbed energies of capsules of different size, composition, and beam selection.

6. Conclusion

The irradiation designs for various capsules were optimized in order to be used for the generation of neutrons in a combined x ray/neutron environment. Due to the number of targets—

one hohlraum and two spherical capsules—each capsule could only utilize 12 of the NIF's 48 quads. The capsules were composed of either glass or plastic, with 1600 µm or 2000 µm diameters. Working with a pre-determined laser pulse shape, the thicknesses of the shells of these capsules were adjusted so that they would implode towards the end of the laser pulse, making use of as much available laser energy as possible. For each capsule, beam pointings and defocuses were varied to determine designs with maximum implosion uniformity. Using hydrodynamic simulations that included 3-D ray tracing, 1-D center-of-mass radius and 3-D center-of-mass profiles were generated to determine optimum uniformity in the vertical and azimuthal directions. Using these designs, it will be possible to irradiate x ray/neutron combined environment targets using only 12 of the NIF's 48 quads for each spherical capsule, with each capsule imploding with an rms nonuniformity of around 3-4%.

7. Acknowledgements

8. References

1. A. M. Cok, "Development of Polar Direct Drive Designs for Initial NIF Targets," Laboratory for Laser Energetics High School Summer Research Program (2006).

2. S. Skupsky, J. A. Marozas, R. S. Craxton, R. Betti, T. J. B. Collins, J. A. Delettrez, V. N. Goncharov, P. W. McKenty, P. B. Radha, T. R. Boehly, J. P. Knauer, F. J. Marshall, D. R. Harding, J. D. Kilkenny, D. D. Meyerhofer, T. C. Sangster, and R. L. McCrory, "Polar Direct Drive on the National Ignition Facility," Phys. Plasmas 11, 2763 (2004).

3. R. S. Craxton, F. J. Marshall, M. J. Bonino, R. Epstein, P. W. McKenty, S. Skupsky, J. A. Delettrez, I. V. Igumenshchev, D. W. Jacobs-Perkins, J. P. Knauer, J. A. Marozas, P. B. Radha, and W. Seka, "Polar Direct Drive: Proof-of-Principle Experiments on OMEGA and Prospects for Ignition on the National Ignition Facility," Phys. Plasmas 12, 056304 (2005).

4. L. A. Tucker, "A Design for a Shock Ignition Experiment on the NIF Including 3-D Effects," Laboratory for Laser Energetics High School Summer Research Program (2011).

5. Dr. Charles Yeamans, Lawrence Livermore National Laboratory, private communication.